



PERFORMANCE OF A RECTANGULAR SECONDARY CONCENTRATOR WITH AN ASYMMETRIC HELIOSTAT FIELD

A. KRIBUS*[†], M. HULEIHIL*, A. TIMINGER** and R. BEN-MAIR*

*Environmental Sciences and Energy Research Department, Weizmann Institute of Science, Rehovot 76100, Israel

**Sektion Physik, Ludwig-Maximilians Universität München, Amalienstr. 54, D-80799 München, Germany

Received 14 June 1999; revised version accepted 22 December 1999

Communicated by LORIN VANT-HULL

Abstract—Secondary concentrators with non-regular cross section have been proposed to permit additional degrees of freedom in heliostat field design, free of the limitations imposed by conventional rotationally symmetric concentrators. A new class of concentrators with a rectangular cross section was found by numerical optimization for heliostat fields having an elliptic contour with high eccentricity. An example of such a rectangular concentrator was constructed and tested at the Weizmann Institute, where the heliostat field has a strong asymmetry and is poorly suited for symmetric (having regular cross section) concentrators. The performance of the new concentrator has been tested using calorimetric and radiometric measurements. The tests were carried out for several heliostats, located in representative positions relative to the predicted acceptance contours of the concentrator. The results of the tests show an agreement with the prediction, and validate the new design for use with highly eccentric fields. A more general conclusion is the validation of the approach of optimizing faceted secondary concentrators with flexible geometry to match heliostat fields having a wide range of possible contours. © 2000 Elsevier Science Ltd. All rights reserved.

1. INTRODUCTION

In solar tower plants with high temperature thermal receivers, secondary concentrators may be used to increase the flux density of the radiation incident on the receiver. The increased flux enhances the receiver efficiency and subsequently the overall system performance by reducing the size of the thermal receiver. In an ideal case where a rotationally symmetric field of heliostats surrounds the tower, an axisymmetric secondary concentrator such as a Compound Parabolic Concentrator (CPC), a tailored reflector (Gordon and Ries, 1993), or a cone (Athavaley *et al.*, 1979; Friedman *et al.*, 1995) are the obvious solutions. For locations at higher latitudes, however, the reflecting area of the heliostats can be used more efficiently if the field of heliostats is located opposite to the sun as seen from the tower, and the field is then asymmetric with regard to the tower. For example, the field is preferably biased towards the north of the tower in case of a location in the northern hemisphere.

Radiation from an asymmetric north-biased

field can be handled in principle by a conventional rotationally symmetric secondary concentrator, whose optical axis is tilted with regard to the ground normal. However, the set of directions intercepted by the secondary concentrator corresponds to the contour of the field. The field contour must then be elliptical, with the large axis pointing in the radial direction, and an eccentricity depending on the tilt angle, as seen in Fig. 1a. However, heliostats should not be placed at large distances from the tower, since distant heliostats produce a larger image of the sun, leading to a reduction in average concentration. Distant heliostats also must be spaced further apart to avoid blocking losses, as compared to heliostats which are closer to the tower. The elongated radial ellipse of Fig. 1a is therefore undesirable. A better deployment providing heliostats close to the tower can be achieved by partitioning the field into several groups of heliostats, each supplying radiation to a separate receiver (Segal and Epstein, 1999). However, the division of the field into elliptical regions resulting from axisymmetric reflectors is not amenable to close packing, and much of the field area is outside of the acceptance range of the concentrators. To accept efficiently radiation with a different distribution of directions corresponding to a complete field without gaps,

[†]Author to whom correspondence should be addressed. Tel.: +972-8-934-3766; fax: +972-8-934-4124; e-mail: avi.kribus@weizmann.ac.il

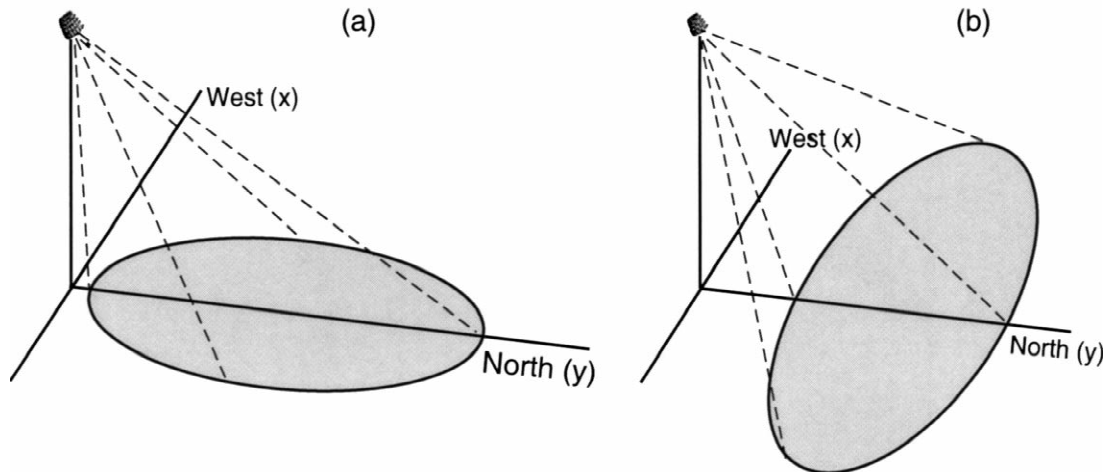


Fig. 1. (a) Elliptical contour of a north-field accepted by an axisymmetric tilted secondary reflector; (b) an east-west wide field, requiring a non-axisymmetric concentrator.

such as shown in Fig. 1b, a non-standard concentrator not conforming to axial symmetry is required (Spirkl *et al.*, 1998; Timinger *et al.*, 2000).

We consider concentrators made of facets, rather than smooth surfaces. Practical concentrators for large-scale systems are usually built from smaller facets, usually as an approximation to a smooth ideal shape such as a CPC (Levy and Epstein, 1998; Miron *et al.*, 1998). Another reason for constructing secondary concentrators from facets is receiver partitioning (Ries *et al.*, 1995; Doron and Kribus, 1996). Partitioning means dividing the secondary concentrator's aperture area at the heliostat field's aim point into several side-by-side apertures, each with a separate concentrator and receiver. The receivers are connected in series, with the fluid heated gradually as it passes through each receiver. This makes a better use of the non-uniform flux distribution available at the aim point of a heliostat field. Partitioning requires that the entrance apertures of the secondary concentrators be matching polygons, to provide complete coverage of the area without gaps. If all apertures are regular polygons, then solutions such as squares and regular hexagons are the natural choices. If irregular polygons are permitted, then the options may be somewhat expanded. Since the apertures are polygonal, it is a natural first approach to construct the entire concentrator from plane facets. Another natural option is facets with one-dimensional curvature (Doron and Kribus, 1996; Timinger *et al.*, 2000); however, this design is more complex and expensive.

We have designed, constructed and tested a concentrator with non-regular cross section, opti-

mized to accept the radiation reflected from a heliostat field that is asymmetric relative to the tower. The available field at the Weizmann Institute corresponds to a strongly asymmetric configuration, a north field with a large east-west angular extent (40° half angle) and a small north-south angular extent (12° half angle). This is very different from the usual elliptic form created by a symmetric acceptance cone and hence is suitable for testing of a non-regular design. The geometry of the new concentrator is a rectangular cross section, the result of an optimization process that considered several concentrator geometry options, with both regular and irregular cross sections (Timinger *et al.*, 2000).

We first discuss the optical design process that produced the new class of concentrators, and then describe the specific concentrator that was built, the experimental system, and the test procedure. The experimental errors and the approximations used in analyzing the results are described in detail. The results and their significance are then presented and discussed.

2. CONCENTRATOR TEST SYSTEM

2.1. Optical design

We have defined faceted concentrators with hexagonal and rectangular cross-section (Fig. 2), having several free parameters that are subject to optimization. The primary field is an ellipse that is wide in the east-west direction as in Fig. 1b, similar to the field at the Weizmann Institute. The performance of each geometry is computed using ray tracing, and the free parameters were varied

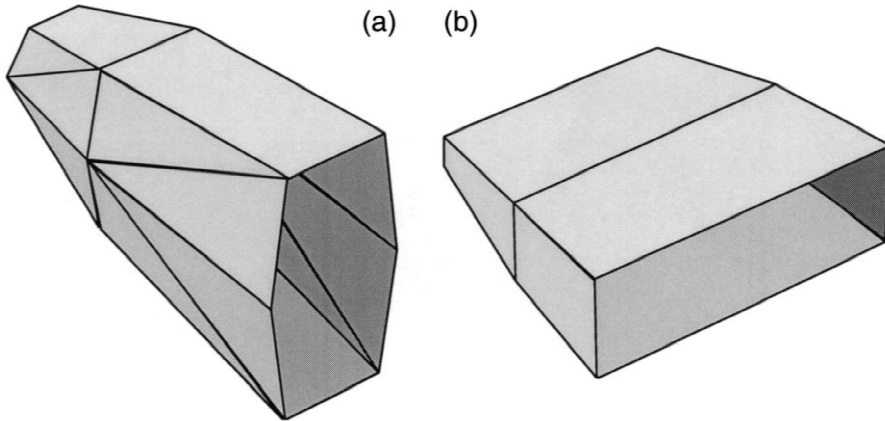


Fig. 2. Optimized non-regular polygonal concentrators. (a) Hexagonal concentrator with an irregular entrance and a regular exit aperture; (b) rectangular concentrator with irregular entrance and exit apertures.

within an optimization process (Spirkl *et al.*, 1998) to provide the highest transmission efficiency. The incident radiation in all cases corresponds to the directional distribution of the full asymmetric field. The non-regular concentrator was optimized under the constraint of fixed aperture area, while the reference regular concentrator was subject to the additional constraint of a regular polygon aperture. The full optical analysis for an asymmetric elliptic field is presented in Timinger *et al.* (1998b, 2000). The optimized rectangular concentrator produced the best performance for the given field. The concentration was about 65% of the thermodynamic limit at 90% transmission efficiency, compared to less than 35% of the thermodynamic limit at the same efficiency for an optimized concentrator limited to regular (square or hexagonal) apertures. This indicates that in theory, it is possible to adapt the secondary concentrator to the characteristics of the incoming radiation, even for a field with strong directional asymmetry.

Concentrators with rectangular exit aperture are not suitable for receivers with a standard circular aperture. However, they may be suitable for open, non-windowed receivers that pose no restrictions on the shape of the aperture. Such open receivers may be used in applications such as industrial process heat. The additional degree of freedom provides a significant performance advantage relative to the regular exit aperture. We have therefore selected the rectangular concentrator of Fig. 2b for experimental demonstration. The theoretical performance of the selected concentrator is: geometric concentration (ratio of entrance to exit aperture area) of 4.5, and transmission efficiency (including absorption and rejection

losses from the whole elliptic field) of 0.927 for mirror reflectivity of 0.95.

2.2. Concentrator construction

The geometry of the rectangular concentrator is shown in Fig. 3. The dimensions, as designed and as manufactured, are given in Table 1. The inlet aperture of the concentrator is small (maximum dimension less than 50 cm), intercepting only a part of the incident flux, corresponding to a central stage of a partitioned receiver system. The single facet measurements were taken on the aluminum base plates before installing the glass mirrors. The assembly measurement was taken on the fully assembled concentrator, and the intermediate aperture was inaccessible for measuring. We note that most of the dimensions were reasonably manufactured, except the length of the two sections. It seems that the two lengths were interchanged, creating a significant error in the slope. This error was clearly observed in a direct optical measurement (Timinger *et al.*, submitted). The effect of these construction errors on the concentrator transmission is relatively small. For heliostat 400, in the center of the field (Fig. 6), the difference in transmission between the ideal geometry and actual geometry is too small to be detected. For heliostat 100, at the edge of the acceptance range, the difference is about 5%.

The concentrator was constructed from flat aluminum sheets, cut and machined to the required dimensions. The reflective surfaces were produced from 0.7-mm-thick glass mirrors, manufactured by Glaverbel from Vertec type glass with a back silver coating. The mirrors were glued to the backing aluminum plates using a 50- μm -thick silicone adhesive tape. Copper tubes (1/4" diam-

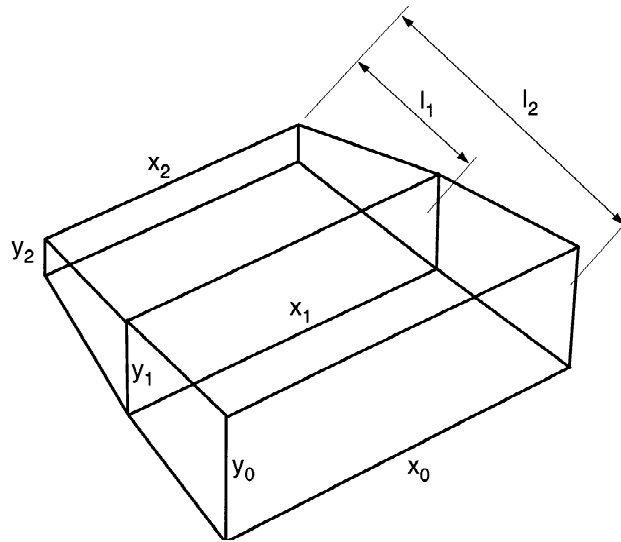


Fig. 3. Geometry of the rectangular concentrator. Dimensions are given in Table 1.

eter) for water cooling were attached to the back of the plates. Thermal contact of the tubes with the plates was obtained by application of a high-conductivity 'Fel-Epoxy' filler. The cooling system was designed to keep the reflector and adhesive temperatures to less than 100°C, to avoid reflector degradation. The concentrator plates were assembled within a frame, which also provides mounting points to the test stand.

2.3. Calorimeter

The calorimeter was designed to accept one or two heliostats at a time; since power is additive, there is no need to measure the entire field simultaneously. The calorimeter was constructed as a cylindrical cavity, with a 1-mm copper sheet forming the cylindrical side wall, and 2-mm copper sheets forming the front and back planes

(Fig. 4). The front cover was made from two semicircular pieces, as shown in Fig. 4b, and a rectangular space between the pieces was designed to match the exit aperture of the concentrator. The interior of the cavity was painted black to maximize absorption. Copper tubes (1/4") for cooling water were soldered adjacent to the outer surface, with high-conductivity adhesive filling the gaps around the tubes to improve heat conduction. The entire calorimeter was covered with synthetic foam insulation sheets and an external aluminum sheet to protect the insulation. The water tubes contain thermocouple wells at the inlet and exit of the calorimeter to permit measurement of the temperature increase across the device. A manual flow meter was installed in the water line leading to the calorimeter. Typical flow rate was about 200 l/h, and temperature differences across the calorimeter were about 5–8 K, leading to absorbed power of about 1–1.5 kW.

2.4. Test station

The test system was installed at the 9th floor of the Weizmann Institute Solar Tower (Fig. 5). Four Ophir model 150W-BNC-Y radiometers are installed around the center of the target, to provide information on the flux distribution on the target. The radiometers measure incident power of up to 100 W, with sensitivity of 0.25 ± 0.004 mV/W. The radiometers are factory calibrated using a YAG laser at 1.064 μm . Spectral variations of the radiometer sensitivity in the solar range are within $\pm 2\%$. Water cooling is supplied to the radiometers

Table 1. Dimensions (in mm) of the rectangular concentrator. Symbols are defined in Fig. 3. Measurement errors in the single facet and assembled concentrator measurements are 0.5 mm and 0.2 mm, respectively

	Design	Single facets measurement	Assembly measurement
x_0	474.7	475.8	474.8
y_0	169.4	170.5	170.8
x_1	430.2	431.4	–
y_1	131.4	132.1	–
x_2	354.3	356.3	356.3
y_2	50.5	51.8	51.4
l_1	207.6	211.5	212.4 ± 1.5
l_2	419.6	419.9	419.2
$l_2 - l_1$	212.0	208.4	206.8 ± 1.5

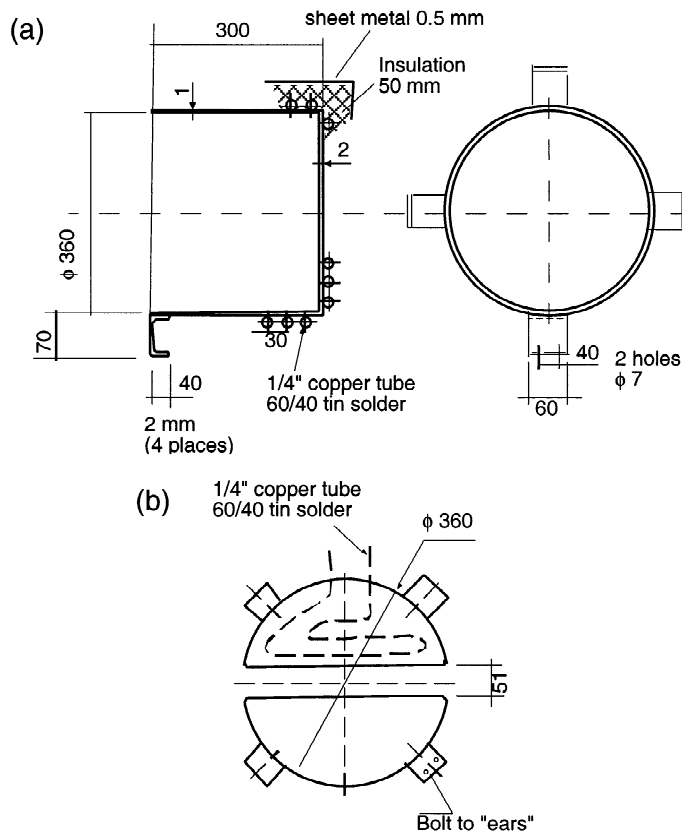


Fig. 4. Design of the calorimeter: (a) cavity, (b) front cover. The exit aperture of the concentrator fits in the rectangular space between the two sections of the front cover.

via a distributor manifold. The temperature of the radiometer body is monitored using a J-type thermocouple.

The calorimeter water inlet and outlet temperatures are measured by J-type thermocouples. The water flow rate is measured by a Manoraz Float Rotameter model KSK, measuring in the range of 100 to 1000 l/h. Water cooling is supplied by the Solar Tower's central closed circuit Receiver Cooling Loop.

The data acquisition system includes two A/D modules. Six thermocouples (four for radiometers, two for the calorimeter) are connected to an ADAM-4018 analog input module. Five analog input signals (four radiometer readings, one insulation value transmitted from the Solar Tower's control room) are connected to a second ADAM-4018 analog input module. The two modules are daisy-chained by an RS-485 communication line to a Pentium 166 PC equipped with a PCL-745-B two-channel RS-422/485 communication card. The input modules read, amplify and translate the signals to engineering units according to software

settings. The interface software running on the PC displays the readings and saves the data to disk.

3. TEST AND DATA ANALYSIS

3.1. Test procedure

Five heliostats were selected for the concentrator test. The positions of these heliostats are shown in Fig. 6. They represent the different regions in the field in terms of theoretical acceptance. Heliostat 400 is in the center of the acceptance range, and should have no rejection. Heliostats 100, 101 and 201 are at the southern edge of the acceptance range, and represent a gradual transition from low to high acceptance. Heliostat 513 is at the western edge, demonstrating the wide acceptance range in the east–west direction.

The test procedure includes the following steps. The heliostat is aimed at the center of the target, and aiming is verified by the field operator (using a video camera observing the target), and by observing the readings of the radiometers installed

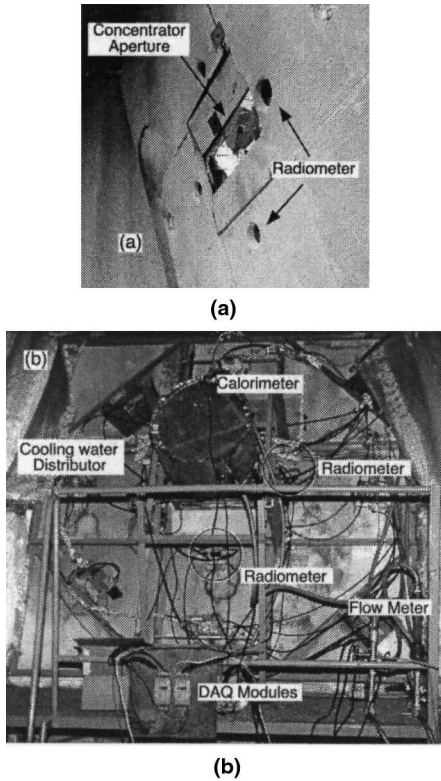


Fig. 5. Concentrator test system. (a) Front, showing radiometer apertures and rectangular concentrator aperture; (b) back, showing the central calorimeter, water cooling system, and data acquisition modules.

symmetrically around the inlet aperture. The power output of the calorimeter is recorded, until achieving thermal steady-state. The next step is mapping the radiation flux incident on the target. The heliostat is moved in small steps in the azimuth and elevation tracking axes. The radiometer readings are recorded at each new position. For each heliostat, four series of data were taken. Each corresponding to one general direction of spot movement: up, down, east and west. These measurements were later analyzed to produce the incident flux (see below). The positions of the measurement points relative to the center of the flux distribution are shown in Fig. 7.

3.2. Radiometer data

The response of the radiometers to the changes of the heliostat aim point is shown in Fig. 8a. The step changes in the average reading are clearly visible, and the average value is nearly constant during the intervals between movements. In some cases the steps were not visible in the data, and we assume that the flux distribution is approximately uniform in these regions.

Within the steady-state intervals there seems to be significant ‘noise’. When we increase the resolution, Fig. 8b, we see that much of the small-scale variation is a periodic change with

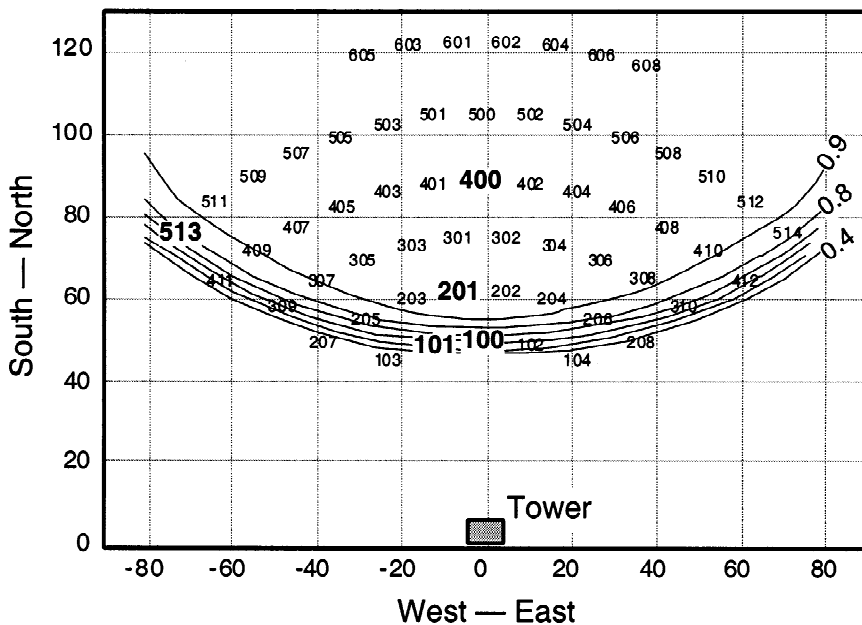


Fig. 6. Positions of heliostats used in the concentrator tests (numbers in boldface). Contours are computed lines of equal transmission efficiency for the rectangular concentrator with reflectivity of 0.95. The central line of the concentrator is aimed roughly at heliostat 400.

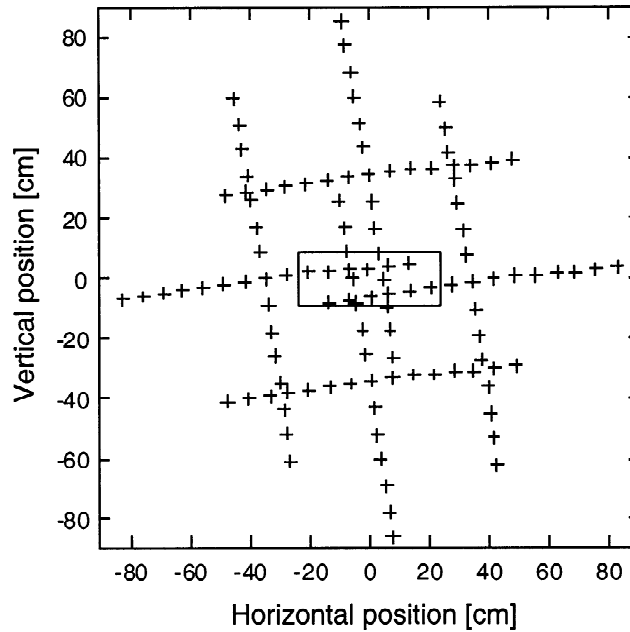


Fig. 7. Position of flux measurement points relative to the central aiming point, as produced by the 'sweeping' procedure (see text). Rectangle at the center is the entrance aperture of the concentrator.

period of about 20 s. This corresponds to the heliostat tracking motion, and is therefore not measurement error but a true physical effect. In the analysis below we average the radiometer readings over each interval of fixed aim point, and the variations due to heliostat tracking are smoothed.

3.3. Flux data processing

We did not have available an instantaneous flux measurement system based on image analysis of a Lambertian target. The flux distribution was therefore constructed from a series of point measurements of the four radiometers. The heliostat aiming point was moved in small steps, such that the radiometers are measuring different portions of the flux distribution after each movement (Fig. 7). The radiometer readings within each steady-state interval between heliostat movements was averaged and normalized to a standard insolation of 800 W/m^2 . The distribution of radiometer readings over the target was fitted to a smooth two-dimensional Gaussian distribution with two different moments and arbitrary orientation of the main axes (Fig. 9). To produce a better fit to the region of interest, the fit was restricted to the data in and close to the entrance aperture. About 35 to 50 data points were used. The maximum deviation of single points was about 10% to 15%. The RMS

deviation is smaller, in some cases down to 2%. The power incident into the concentrator aperture was then calculated by integrating the smooth fitting function. The transmission efficiency is the calorimeter power output (also normalized to insolation of 800 W/m^2) divided by the incident radiative power.

3.4. Calorimeter data

The calorimetric measurement was repeated four times, with the heliostat aimed at the center of the target before each flux distribution scan as described above. In principle, all four measurements should be the same. In fact, there are significant differences among the results (Fig. 10). Changes in insolation were neutralized by normalizing both radiometer and calorimeter data to a standard insolation of 800 W/m^2 . The small instability in each time series (jumps of about 0.05 kW) is due to the resolution of the thermocouple data acquisition. The differences among the four results is larger than the thermocouple experimental error. The reason for this difference is probably the deformation of the spot on the target due to a time-dependent astigmatic effect.

Each of the four measurements was analyzed separately. However, the complete flux distribution is produced by accumulation of all four scans of the heliostat aim point; therefore the four

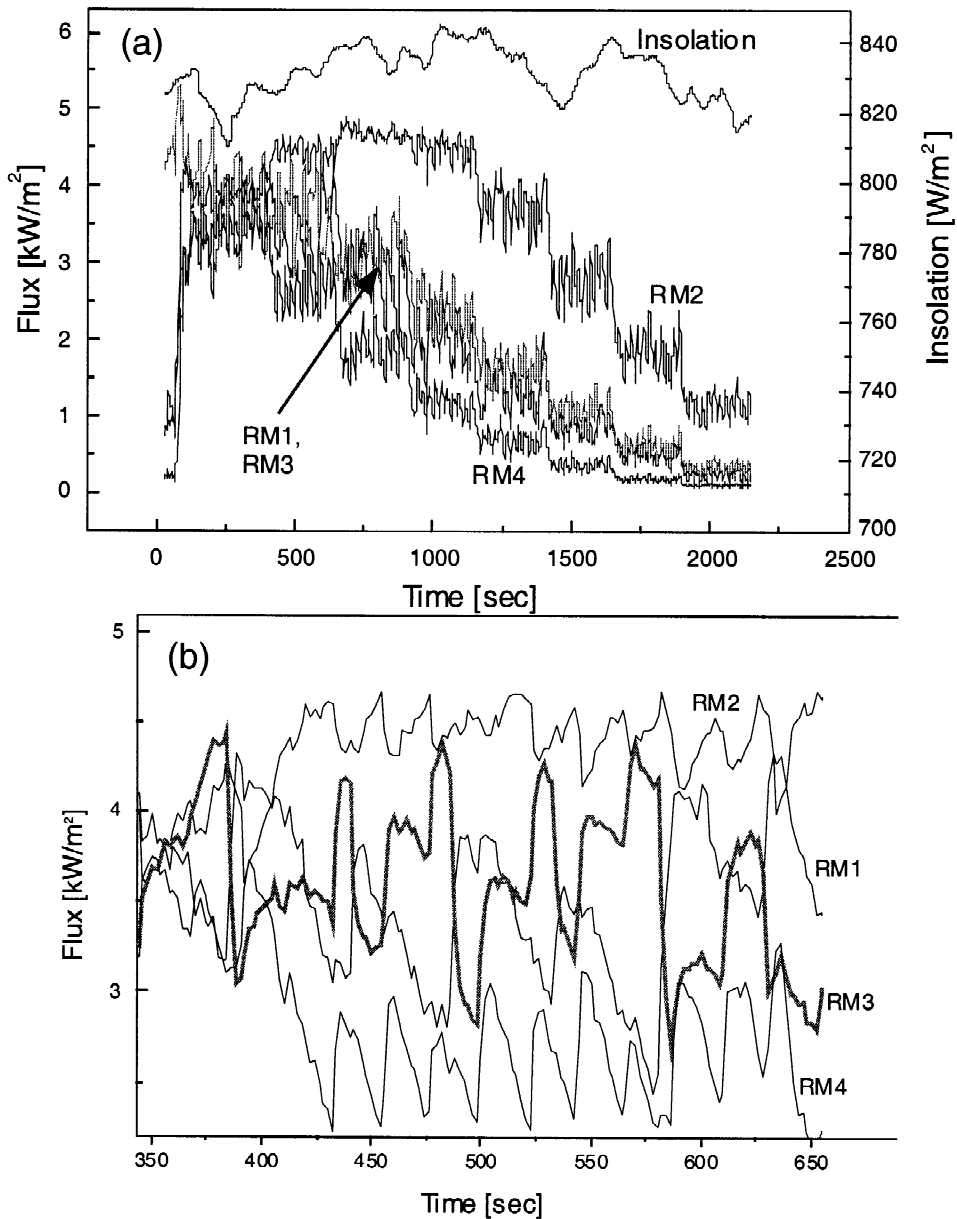


Fig. 8. Response of radiometers to movement of the aim point. (a) Large scale motions of changing the heliostat aim point; (b) small scale motions of heliostat automatic tracking.

different calorimeter measurements are compared to a single averaged prediction based on the common flux distribution.

3.5. Measurement error analysis

3.5.1. Concentrator reflectivity. We measured the absorbed power in the concentrator due to imperfect reflectivity, surface contamination and damage, and gaps between the reflective elements,

using the cooling circuit of the concentrator as a calorimeter. The cooling load was measured for different flow rates of the water in the cooling circuit. The readings were plotted and extrapolated to an infinite value of the water flow rate, corresponding to zero temperature difference (Fig. 11). This should take into account the heat that was absorbed in the reflector but lost to other possible heat sinks, such as the conduction to the calorimeter or convection and thermal radiation to

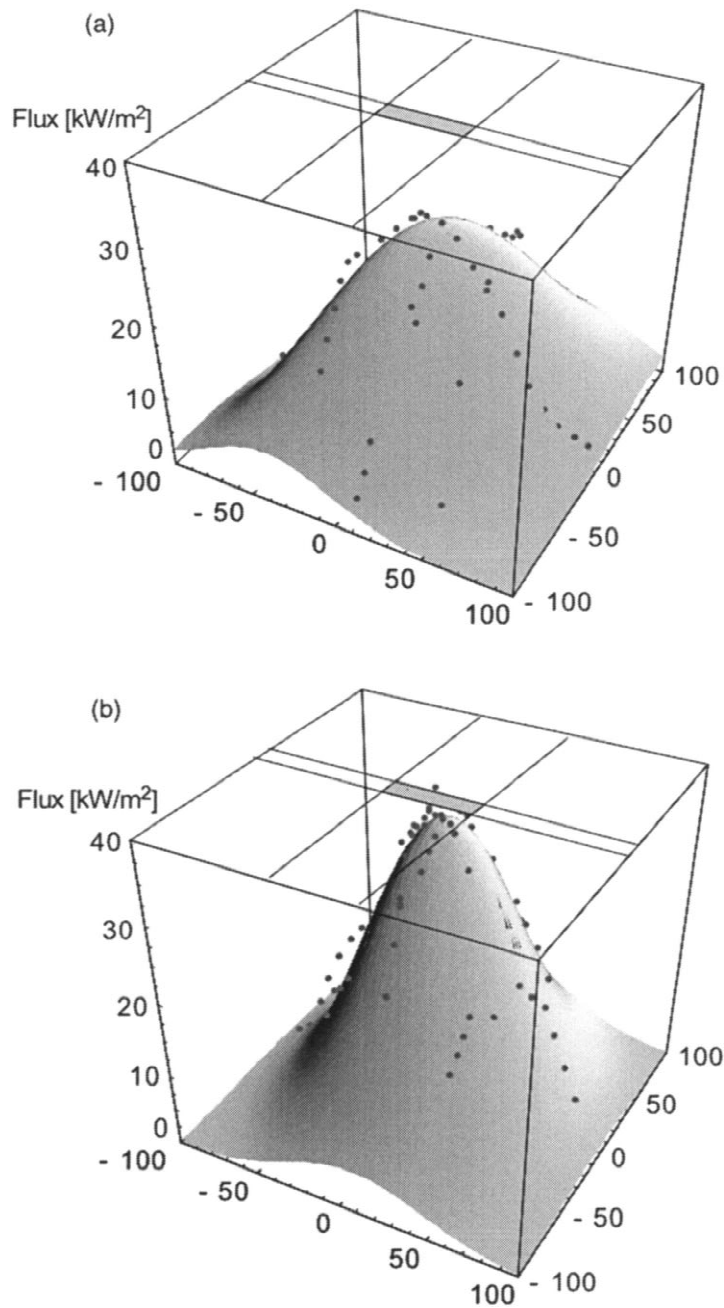


Fig. 9. Flux distribution of (a) heliostat 100 and (b) heliostat 201. The dots are the measured, averaged and scaled radiometer data; the surface is the fitted Gaussian function. Some of the data dots are hidden below the surface. The lines on the top surface indicate the extent of the concentrator inlet aperture. Target dimensions are in centimetres.

the environment. The measurements were repeated with and without thermal insulation over the concentrator's external surfaces. Both measurements lead to the same result: absorptive losses in the concentrator are about 24%. Since the ray tracing simulation indicates that the average number of reflections is about one, we set the

actual average reflectivity of the concentrator surfaces to 0.76. This is much lower than the expected reflectivity of 0.9–0.94. In future concentrators the higher values should be achievable, using better handling and installation procedures to avoid the reflector damage that was observed in this concentrator.

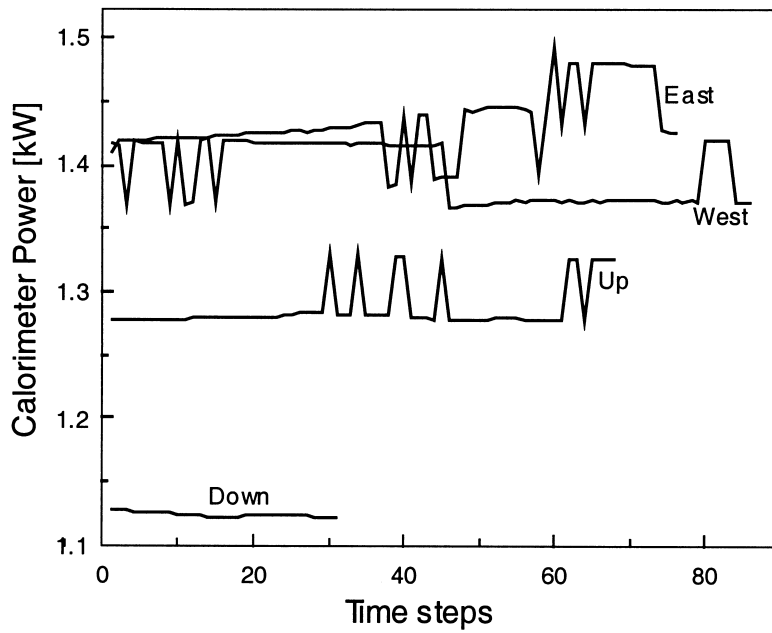


Fig. 10. Calorimeter output for heliostat 513 aimed at the center of the concentrator, at four different times.

3.5.2. Radiometer effective area. The radiometer was originally designed for laser applications, where the light is nearly collimated, and is carefully controlled to arrive only within the black absorbing disc that constitutes the sensor element. In solar tests with concentrated sunlight, the radiation arrives within a wide range of angles and over a wide area. Interpretation of the power reading to provide the flux therefore needs to take

into account the effective measurement area, which might include for example the conical walls surrounding the sensor disc.

The radiometer behavior under heliostat radiation was checked by positioning stops of different sizes in front of the radiometer and plotting the readings versus the stop opening area. The results are shown in Fig. 12 for two solar tests and one test with a strong halogen lamp. The radiometer

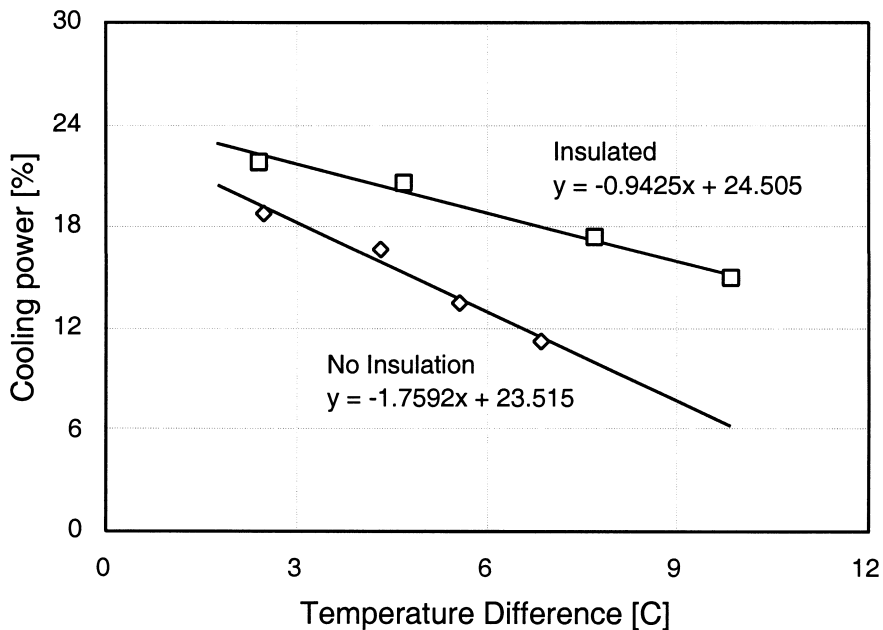


Fig. 11. Calorimetric measurement of the concentrator absorption loss.

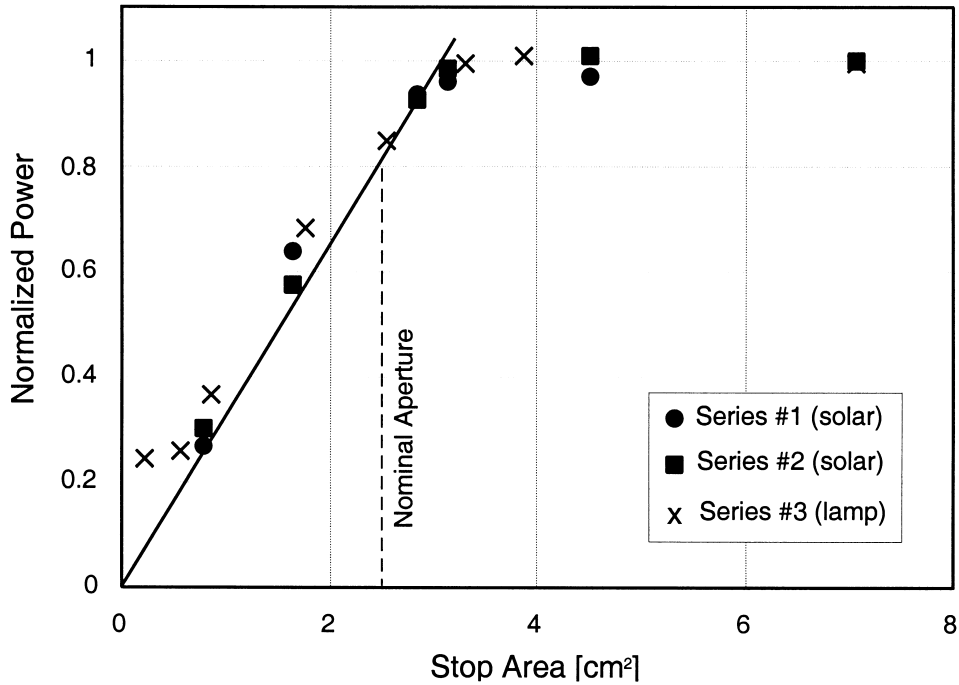


Fig. 12. Variation of relative radiometer reading (normalized to maximum reading when completely exposed), as a function of the aperture stop area, for two solar tests and a test with a halogen lamp.

reading keeps increasing when the stop size is increased beyond the nominal size of the sensitive area of the radiometer (2.54 cm^2). This signifies that radiation absorbed in the surfaces surrounding the sensitive area of the radiometers makes additional thermal contributions which are included in the measurement. An effective sensitive area of the radiometers was determined out of the maximum stop size that still contributed to the radiometer readings. The effective area is by a factor of 1.25 bigger than the nominal sensitive area.

We have discovered after the tests that for Heliostat 513, the radiometer aperture opening was partly shaded by the front plate. The effect was eliminated by adjusting the effective area for the calculation of the flux by the shading ratio.

3.5.3. Calorimeter thermal loss. A possible experimental error exists if there is excessive thermal loss from the calorimeter walls to the environment, by conduction, convection or thermal radiation. This loss was minimized by installation of thermal insulation around the calorimeter, and operating as close as possible to room temperature (temperature rise of the cooling water is usually only a few degrees). To verify that these measures are sufficient, we checked the variation of the calorimeter power with water flow rate, and extrapolated to infinite flow rate which

corresponds to zero temperature difference and presumably zero loss to the environment, similar to the procedure used for the concentrator loss (see above). The variation of power with flow rate was found to be negligible, and the extrapolated value corresponding to infinite flow rate is well within the range of the measured results for finite flow rates. We conclude then that the thermal loss from the calorimeter is insignificant.

3.5.4. Cumulative measurement errors. Each quantity measured in the tests introduces a certain amount of error. We have estimated lower and upper bounds on the relative error for the major error sources. These estimates are based on the manufacturers' specifications and on the amount of noise in the actual readings. The estimates are summarized in Table 2. The total error for the measured power is derived by the sum-of-squares

Table 2. Experimental relative error estimates for the concentrator tests

Relative errors	Minimum	Maximum
Measured power		
Calorimeter water flow rate	0.02	0.04
Calorimeter temperature rise	0.01	0.03
Radiometer effective area	0.08	0.12
Analytic match to flux distribution	0.07	0.18
Total error	0.11	0.22
Simulated power		
Reflector absorption loss	0.02	0.05

rule. For the simulation results (see next section), the statistical error due to ray tracing is small ($< 1\%$) and the main error source is due to the uncertainty in the mirror reflectivity and the absorption loss.

4. RESULTS

The transmission of radiation coming from each heliostat was calculated with ray tracing. The dimensions of the reflector were assumed to be as measured using our optical in-situ remote measurement technique (Timinger *et al.*, 1998a, submitted). The reflectivity of the mirrors in the ray tracing calculation was set to 0.76, corresponding to the result of the calorimetric measurement of the concentrator absorption loss.

Fig. 13 presents a comparison of the transmission efficiency for the five tested heliostats, showing the experimental vs. simulated data results. For each heliostat we have four experimental measurements and one simulation prediction based on the composite flux distribution. The error bars in the figure correspond to an intermediate value between the error bounds shown in Table 2: 17% for the measurement, 3% for the simulation data.

In most cases, the measured values shown in Fig. 13 were somewhat lower than the prediction, but most of the simulated values are within the measurement error bars. This deviation to somewhat lower values is probably related to our

inaccurate procedure for measuring the flux distribution, which is a composite of several successive measurements over time rather than an instantaneous ‘snapshot’. However, the measured results correctly reproduce the predicted trend, indicating that the optical analysis is essentially correct.

5. DISCUSSION

We have demonstrated a novel concentrator with strongly asymmetric acceptance in directional space, corresponding to the east–west wide field that is available at the Weizmann Institute. Such an acceptance range cannot be achieved with axisymmetric concentrators such as a CPC or TERC, without sacrificing either concentration ratio or transmission efficiency.

We have measured the transmission efficiency of the novel secondary concentrator using calorimetry. The experimental results were close to the predictions by ray tracing simulation, usually within experimental error and qualitatively producing the expected trend. The quality of the measurement was not high, mostly due to inaccuracy in the measurement of the incident flux distribution. Nevertheless, we were able to reproduce the desired trends and transmission efficiency values and to demonstrate the new non-regular concentrator design.

The construction of the new concentrator design is relatively simple. It is made from a small

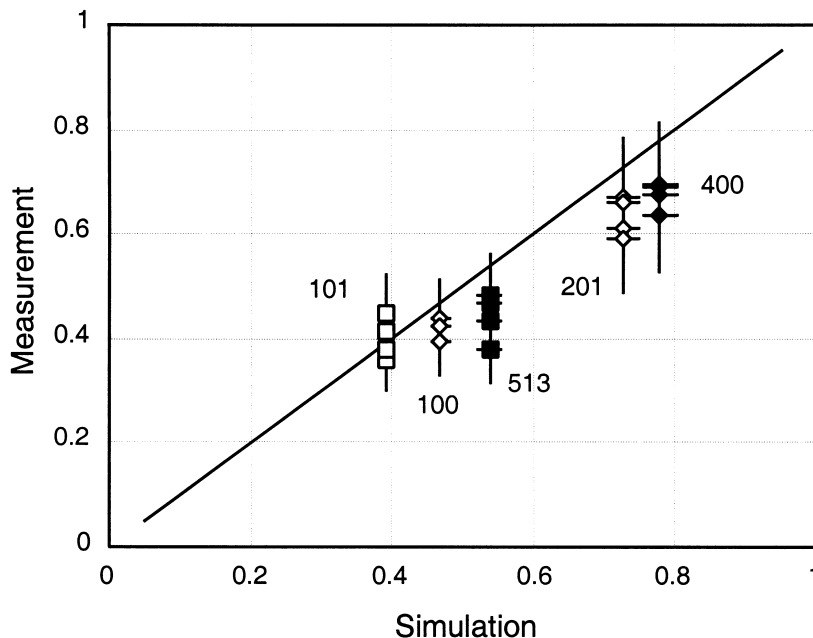


Fig. 13. Measured vs. simulated transmission efficiency for the five heliostats. Diagonal line indicates an exact match.

number of flat facets, which can be easily manufactured within a wide range of sizes. The assembly and framing of the concentrator are also simple due to the rectangular cross-section, with no need for complex three-dimensional structures. This is much simpler than traditional concentrators that attempt to approximate an axisymmetric CPC with many small facets (Buck *et al.*, 1998; Levy and Epstein, 1998). The rectangular concentrator is therefore a practical and relatively low-cost solution for central receiver systems, in addition to its optical advantages.

The significance of this demonstration is not just for this particular field layout. An appropriate non-regular optical solution can be derived for many types of asymmetric fields using the optimization procedure presented by Timinger *et al.* (1998b). The severe restrictions placed on high-performance field design by symmetric secondary concentrators are therefore alleviated, and additional degrees of freedom are now available for field design and optimization.

Acknowledgements—The contributions made by I. Levy and Y. Adikman are gratefully acknowledged. This research was supported by a grant from the German Federal Ministry of Education, Science, Research and Technology (BMBF) and the Israeli Ministry of Science (MOS) under the aegis of KFA-BEO-Forschungszentrum Jülich GmbH/Projekträger für Biologie, Energie, und Ökologie.

REFERENCES

- Athavaley K., Lipps F. W. and Vant-Hull L. L. (1979) An analysis of the terminal concentrator concept for solar central receiver systems. *Solar Energy* **22**, 493–504.
- Buck R., Abele M., Kunberger T., Denk T., Heller P. and Lüpfert E. (1998) Receiver for solar-hybrid gas turbine and combined cycle systems. In *9th International Symposium Solar Thermal Concentrating Technologies, Odeillo*, EDP Sciences.
- Doron P. and Kribus A. (1996) Receiver partitioning: a performance boost for high-temperature solar applications. In *8th International Symposium Solar Thermal Concentrating Technologies, Köln*, Vol. 2, pp. 621–630.
- Friedman R. P., Gordon J. M. and Ries H. (1995) V-cones as secondary concentrators in high-flux solar designs: the overlooked gem. In *Proceedings ISES Solar World Congress, Zimbabwe*.
- Gordon J. M. and Ries H. (1993) Tailored edge-ray concentrators as ideal second stage for Fresnel reflectors. *Appl. Optics* **32**, 2243–2251.
- Levy I. and Epstein M. (1998) Design and operation of a high-power secondary concentrator. In *9th International Symposium Solar Thermal Concentrating Technologies, Odeillo*, EDP Sciences.
- Miron G., Weis S., Anteby I., Taragan E. and Sagie D. (1998) A large Compound Parabolic Concentrator for 500 kWth solar central receiver system: design and evaluation. In *9th International Symposium Solar Thermal Concentrating Technologies, Odeillo*.
- Ries H., Kribus A. and Karni J. (1995) Non-isothermal receivers. *J. Solar Energy Eng.* **117**, 259–261.
- Segal A. and Epstein M. (1999) Comparative performance of tower top and tower reflector central solar receivers. *Solar Energy* **65**, 207–226.
- Spirkl W., Timinger A., Ries H., Kribus A. and Muschawek J. (1998) Non-axisymmetric reflectors concentrating radiation from an asymmetric heliostat field onto a circular absorber. *Solar Energy* **63**, 23–30.
- Timinger A., Smith T., Walther M., Spirkl W., Kribus A., Ries H. and Doron P. (1998a) Optical in-situ analysis of secondary reflectors in solar tower plants. In *9th International Symposium Solar Thermal Concentrating Technologies, Odeillo*, pp. 117–122, EDP Sciences.
- Timinger A., Spirkl W., Kribus A. and Ries H. (1998b) Asymmetric secondary reflectors for multi-stage solar tower plants. In *9th International Symposium Solar Thermal Concentrating Technologies, Odeillo*, pp. 111–115, EDP Sciences.
- Timinger A., Kribus A., Ries H., Smith T. and Walther M. Optical assessment of nonimaging concentrators. *Applied Optics* (submitted).
- Timinger A., Spirkl W., Kribus A. and Ries H. (2000) Optimized secondary concentrators for a partitioned central receiver system. *Solar Energy* **69**, 153–162.